JACS
JOURNAL OF THE AMERICAN CHEMICAL SOCIETY
Article
pubs.acs.org/JACS

Selective Formation of Hydrogen and Hydroxyl Radicals by Electron Beam Irradiation and Their Reactivity with Perfluorosulfonated Acid Ionomer

Lida Ghassemzadeh, Timothy J. Peckham, Thomas Weissbach, Xiaoyan Luo, and Steven Holdcroft*

Department of Chemistry, Simon Fraser University, 8888 University Drive, Burnaby, British Columbia, Canada V5A 1S6

Supporting Information

ABSTRACT: Selective formation and reactivity of hydrogen ($H^{\bullet}$) and hydroxyl ($HO^{\bullet}$) radicals with perfluorinated sulfonated ionomer membrane, Nafion 211, is described. Selective formation of radicals was achieved by electron beam irradiation of aqueous solutions of H_2O_2 or H_2SO_4 to form $HO^{\bullet}$ and $H^{\bullet}$, respectively, and confirmed by ESR spectroscopy using a spin trap. The structure of Nafion 211 after reaction with $H^{\bullet}$ or $HO^{\bullet}$ was determined using calibrated ^{19}F magic angle spinning NMR spectroscopy. Soluble residues of degradation were analyzed by liquid and solid-state NMR. NMR and ATR-FTIR spectroscopy, together with determination of ion exchange capacity, water uptake, proton conductivity, and fluoride ion release, strongly indicate that attack by $H^{\bullet}$ occurs at the tertiary carbon C−F bond on both the main and side chain; whereas attack by $HO^{\bullet}$ occurs solely on the side chain, specifically, the α-O−C bond.

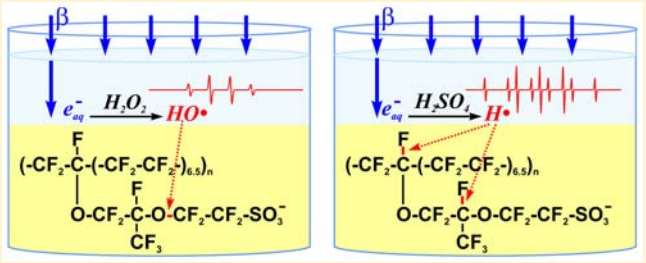

INTRODUCTION

Proton exchange membrane fuel cells (PEMFCs) continue to attract attention in a range of applications, including automotive, portable, and stationary power, and personal electronic devices.[1,2] However, an area of technological concern is the less-than-desirable durability of commercially available PEMs. Even "chemically resistant" perfluorosulfonic acid (PFSA) ionomers are prone to failure before the minimum lifetime requirements for automotive and stationary power generation, respectively.[3,4]

Mechanical degradation of the membrane occurs under normal fuel cell operating conditions due to repetitive swelling and shrinking, caused by variations in membrane temperature and humidity.[5] Mechanical degradation is vastly exacerbated by chemical degradation of the ionomer which results in a reduction in ion exchange capacity,[6] pH,[7] proton conductivity,[7,8] and membrane thickness, together with an increase of fluoride ion release.[7,9−16]

Chemical degradation is believed to be initiated by the formation of highly reactive free radicals. In situ ESR studies on Nafion PFSA ionomer membranes have identified three different radicals at the anode and the cathode: hydroxyl ($HO^{\bullet}$), hydroperoxyl ($HOO^{\bullet}$), and hydrogen ($H^{\bullet}$).[17] There is a lack of concensus on their origin as they can originate electrochemically and/or chemically at either the anode or the cathode.[17−19] Two pathways commonly discussed are the electrochemical generation of hydroperoxide and its subsequent cleavage by thermolysis or transition metal catalysis,[7,17,19,20] and the chemical generation of radicals by direct reaction of $H_2(g)$ and $O_2(g)$ on Pt, which occurs upon oxygen and/or hydrogen crossover.[9,13,15,18,21,22]

Ex situ studies of membrane degradation have played an important role in the development of PEMs as they provide details on degradation pathways and hence provide strategies for degradation mitigation. For instance, it was qualitatively deduced that early versions of PFSA ionomer degrades by reaction of hydroxyl/hydroperoxyl radicals with terminal groups on the main chain (e.g., −COOH, $-CF_2H$, $-CF{=}CF_2$)[23−26] and $-OCF_2-$ and $-CF_2SO_3^-$ groups on the side chain.[18,24,25,27−34] The former degradation pathway was effectively eliminated upon chemical modification of the main chain termini by postfluorination.[18,24,25,30−34] Structural elucidation of stabilized Nafion 211 after an ex situ Fenton's reagent test confirmed that the first point of $HO^{\bullet}$ radical attack occurs at the side chain α-O−C bond, leading to cleavage of $-CF_2-CF_2SO_3^-/-OCF_2-CF_2SO_3^-$ (Scheme 1).[34] However, Fenton's reagent tests produce a mixture of $HO^{\bullet}$ and $HOO^{\bullet}$ radicals[31,35,36] while half-fuel cell arrangements generate a mixture of $HO^{\bullet}$, $HOO^{\bullet}$, and $H^{\bullet}$.[9,15,18] Thus, different radicals

Scheme 1. Chemical Structure of Nafion 211 and Group Assignments Used in This Work[a]

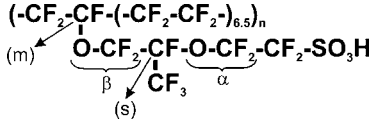

[a](m) and (s) are used to differentiate main chain from side chain.

Received: August 3, 2013
Published: September 27, 2013

   dx.doi.org/10.1021/ja408032p | J. Am. Chem. Soc. 2013, 135, 15923−15932

are produced by different methods and radical types are not produced selectively in any currently deployed ex situ method. The selective formation and induced reactivity of single radical species is necessary in order to further understand degradation reactions.

Recently, the group of Nishijima reported γ-irradiation of Nafion 117 membranes and noted greater amounts of degradation in the presence of water. This led to speculation that the rate of degradation is enhanced by radicals produced via the radiolysis of water.[15,18,37,38] The same group attempted to generate $HO^{\bullet}$, $H^{\bullet}$, and $O_2^{\bullet-}$ radicals exclusively by γ-irradiation of N_2O-saturated water, Ar-saturated acid (pH 2), and O_2-saturated water, respectively.[39] The membranes were characterized for proton conductivity, while molecular evidence for polymer degradation was restricted to fluoride and sulfate ion release. The mole ratio of eluted carbon to sulfur was shown to be related to the type of radical generated and the different locations of bond cleavage.[39] Despite these creative attempts to selectively generate radicals, no evidence confirming the exclusive formation of desired radicals was provided. Our attempts to reproduce the conditions published indicate that a mixture of radicals is present in all the solutions (see Supporting Information, Figure S1 and S2). Also, due to the high penetration depth of γ-rays, the possibility of membrane degradation by direct irradiation cannot be ignored.

In this work, we build upon the concept of water radiolysis as a technique for selectively producing radicals;[40] but rather than γ-irradiation, we use β-irradiation (e-beam) for which the penetration depth is a function of solvent density/depth,[41] making it possible to control the penetration depth of the beam and thus minimize direct irradiation of the polymer membrane, as shown in Figure 1. More importantly, we demonstrate

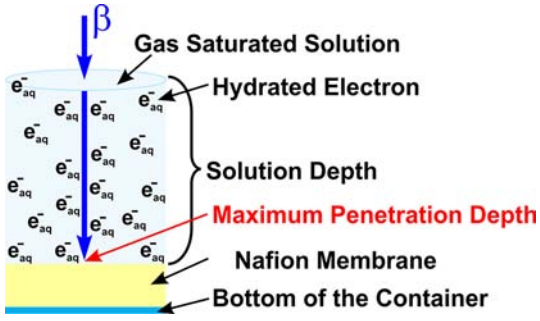

Figure 1. β-irradiation of water. The depth of water was chosen so that hydrated electrons formed, and thus radicals formed, occurred close to the membrane's surface.

selective production of either $HO^{\bullet}$ or $H^{\bullet}$ radicals by reaction of additives with the β-irradiation-generated hydrated electrons according to the reactions below.[40]

Ar-saturated aqueous solutions of H_2O_2:

$$e_{aq}^- + H_2O_2 \rightarrow HO^{\bullet} + HO^- \quad (k = 1.1 \times 10^{10}\,\mathrm{L.\ mol^{-1}s^{-1}})$$

Ar-saturated aqueous acidic solutions (pH 2):

$$e_{aq}^- + H^+ \rightarrow H^{\bullet} \qquad (k = 2.3 \times 10^{10}\,\mathrm{L.\ mol^{-1}s^{-1}})$$

In order to confirm the generation of selective radicals, radicals were captured by a spin trap and detected by ESR spectroscopy. An archetypal, chemically stabilized PFSA ionomer, Nafion 211, was selectively exposed to $H^{\bullet}$ or $HO^{\bullet}$ radicals and the membranes were structurally analyzed in order to distinguish the mechanisms of $H^{\bullet}$ and $HO^{\bullet}$ radical attack. $H^{\bullet}$ and $HO^{\bullet}$ radicals are found to initiate profoundly different pathways of polymer degradation.

EXPERIMENTAL SECTION

Chemicals. All materials were used as received unless otherwise noted. DuPont Nafion 211 (NRE211) was provided by Ballard Power Systems Inc. 30 vol% H_2O_2 (Caledon Laboratory Chemicals Ltd.) and 98% sulfuric acid (Anachemia) were diluted to 10 vol% and 0.01 M, respectively using Milli-Q (18 MΩ) water. 5,5-Dimethyl-1-pyrroline-*N*-oxide (DMPO) was obtained from Santa Cruz Biotechnology Inc.; *t*-butanol (*t*-BuOH), trichlorofluoromethane (CCl_3F), and sodium hexafluorosilicate (Na_2SiF_6) were purchased from Sigma-Aldrich Co. Total ionic strength adjustment buffer (TISAB II, with CDTA) solution was purchased from Thermal Orion. Argon 99.998% (Ar) was purchased from Praxair Technology Inc.

Sample Preparation. Stock solutions for selectively generating radicals were made by sparging a solution with Ar gas overnight. The solutions were either Ar-sparged 10 vol% H_2O_2 for $HO^{\bullet}$ radical formation or Ar-sparged 0.01 M H_2SO_4 (containing 1 M *t*-BuOH) for $H^{\bullet}$ radical formation. *t*-BuOH served to trap any $HO^{\bullet}$ radicals formed.[40,42] Sparging with argon removed oxygen and eliminated formation of $O_2^{\bullet-}$, $O_2^{\bullet 2-}$, and $HOO^{\bullet}$ radicals.

Nafion 211 membranes cut to 6 cm × 6 cm and X-cut in the center to allow gases to escape from beneath the membrane, were kept in a N_2 drybox and placed in individual jars. The membranes were held in place with glass rings (see Figure 2). In an inert Ar atmosphere

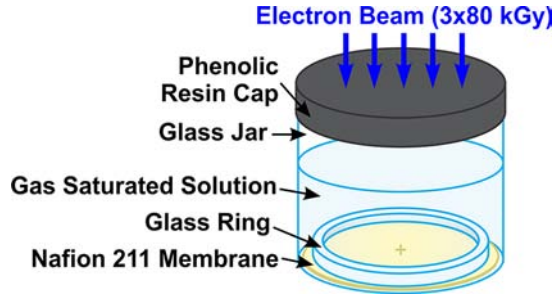

Figure 2. Experimental setup for β-irradiation and generation of radicals.

glovebag 300 mL of solution (chosen according to the desired radical) was poured into each jar to a solution height of 5.8 ± 0.05 cm and sealed with a phenolic resin cap (stable to 100 MGy irradiation). Membranes were immersed for a period of at least 12 h prior to irradiation. The jars were stored under ice to increase the solubility of Ar in the solutions. A minimum of 3 samples of Nafion 211 were used for each radical examined. For ESR experiments, 10 mL of each solution and 0.1 mL of DMPO were added to a 15 mL vial and sealed with a phenolic cap, inside an inert Ar atmosphere glovebag. A minimum of 2 samples of DMPO solutions were used per radical type. ESR samples were prepared shortly before the irradiation to limit decomposition of DMPO.

Irradiation Procedure. E-beam irradiation of samples was carried out at Iotron Industries Canada/USA Inc., Port Coquitlam, BC, Canada, using an IMPELA Electron Beam Accelerator configured for 10 MeV irradiation. IMPELA uses an L-band, on-axis-coupled, standing-wave cavity system for accelerating electrons. Sample containers containing the membrane (or DMPO solutions) were placed on trays and surrounded by ice up to the top of the lid. Irradiation was carried out by passing the samples through the e-beam to acquire a dose of 80 kGy. This process was repeated twice more for a total dose of 240 kGy per sample. In between passes, additional ice was added to ensure that the jars were kept cold. After irradiation, the jars were stored under ice. Irradiated membranes were washed with DI

dx.doi.org/10.1021/ja408032p | J. Am. Chem. Soc. 2013, 135, 15923−15932

water and cut into smaller pieces for analysis. Post-irradiated solutions were analyzed for fluoride ions and by ^{19}F NMR spectroscopy.

The depth of water through which electrons pass before reaching the membrane was chosen to be 5.8 ± 0.05 cm. This was based on the specifications provided by Iotron Industries (Figure 3) stating that

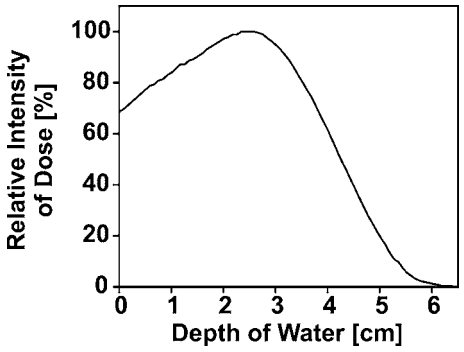

Figure 3. Penetration depth of β-rays using a 10 MeV e-beam source. Data supplied by Iotron Industries Canada/USA Inc. and confirmed by literature data.[43−45]

hydrated electron formation (and hence radical formation) falls to negligible values for path lengths >5.8 cm. At a 5.8 cm depth, less than 2% of the incident irradiation reached the submerged membrane. Our control experiments showed that, when the depth of water was 6 cm or greater, no membrane degradation was observed.

Spin Trap Electron Spin Resonance (ESR) Spectroscopy. ESR spectroscopic analysis was performed on the DMPO solutions within 3 h of irradiation. Spin-trapping was used due to the low concentration and transient nature of the radicals.[46−48] DMPO was chosen because of its well-documented trapping ability (see Supporting Information, Scheme 1).[17,36,49−51] DMPO is known to contain impurities that are difficult to remove. In order to take impurities into account, a pre-irradiated sample of DMPO in water was used as a background signal. For each sample, an ESR X band aqueous flat cell was filled with solution and inserted into the ESR resonator. All ESR experiments were run with identical parameters using the same number of scans. A Bruker ESR spectrometer was used operating at 9.7 GHz and 100 kHz magnetic field modulation, operated by the Bruker BioSpin data system. The acquisition parameters for the experiments were as follows: sweep width, 150 G; microwave power, 2 mW; time constant, 10.24 ms; conversion time, 20 ms; number of data points, 1024; modulation amplitude, 2 G; receiver gain, 1×10^5; and number of scans, 16. Simulation of the spectra was carried out using the ESR public software tool, WinSIM version 0.96.

Solid State ^{19}F Nuclear Magnetic Resonance Spectroscopy. Solid state ^{19}F NMR was performed on Nafion 211 samples before and after irradiation, and on solid residues suspended in solution, if any. NMR analyses were performed at 376.09 MHz on a Bruker 400 MHz spectrometer operating with a static magnetic field of 9.4 T. A 2.5 mm three-channel HFX wide band MAS probe with a Vespel spinning module and zirconia rotors with Vespel drive tips and caps were used in order to avoid fluorine background signals. The spectra were recorded at 300 K, at a spinning rate of 30 kHz, a 90° pulse length of 3.0 μs, a recycle delay of 3 s, and a dwell time of 5 μs. 256 transients were recorded. Each transient was acquired for 4096.24 ms with a spectral width of 227 kHz (~600 ppm). The spectra were processed with TOPSPIN software (Bruker), and the FID was Fourier transformed without any additional line broadening. The chemical shifts were calibrated with respect to Na_2SiF_6 as an external standard having resonance at −151.45 ppm. Quantification of solid ^{19}F NMR data was reported in detail in our recent publication.[34] Briefly, ^{19}F solid state NMR analyses was performed on mixed powders of Na_2SiF_6 (^{19}F-rich) and SiO_2 (^{19}F-free) with different mass ratio. The collected spectrum of each sample was divided by the sample mass to an accuracy of 1 μg and a calibration curve was constructed using the area of the Na_2SiF_6 signal as a function of fluorine concentration. The absolute integrals of each spectrum were normalized to the sample mass and deconvoluted using the *dmfit* program.[52] The area of each peak was related to the fluorine mass using the reference calibration curve.

Liquid and Solid State ^{19}F NMR Spectroscopy of Irradiated Solutions. Membrane residues suspended in solution after irradiation were concentrated by freeze-drying: 35 mL of solution was placed in a 50 mL centrifuge tube. The solution was frozen using liquid nitrogen and transferred to vacuum line of 120 mbar where it remained at −40 °C for at least 48 h. The dehydration process at low temperature and pressure causes the water to sublimate, leaving behind a solid residue. From each post-irradiation solution, 3 samples (3 × 35 mL) were prepared by this technique. After thawing, 1 mL of isopropyl alcohol (IPA) was added to each dried centrifuge tube. The alcohol solutions were then transferred to a 5 mm NMR tube. NMR analyses of solutions were performed at 470.59 MHz on a Bruker 500 MHz spectrometer operating at a static magnetic field of 11.7 T. A double resonance broad band probe was used. ^{19}F NMR spectra were recorded using a 1D sequence with power-gated proton decoupling; a 90° pulse length of 13.5 μs and a recycle delay of 1 s. 8192 transients were recorded. Each transient was acquired for 349.5 ms with a spectral width of 188 kHz (~400 ppm). The spectra were processed with TOPSPIN software (Bruker). The chemical shifts were calibrated with respect to $CClF_3$—an external standard with a resonance at 0 ppm.

^{19}F MAS NMR was used to analyze solid residue present after freeze-drying in a similar manner to that samples described above. The residue was mixed with SiO_2 (as filler) and packed in a 2.5 mm zirconia rotor. The experimental conditions were identical to those used to analyze membranes except a higher number of transactions (8192) was used to improve the signal-to-noise ratio.

Attenuated Total Reflection Infrared (ATR-IR) Spectroscopy. ATR-FTIR spectra were measured with a Nicolet Nexus 670 spectrometer using a single reflection germanium crystal. Spectra were recorded at a resolution of 2 cm^{-1}. The membranes were squeezed between the top surface of a germanium crystal and the ATR-tip. 64 scans were averaged covering a spectral range of 700 to 4000 cm^{-1}.

Fluoride Ion Concentration. The fluoride ion concentration released from the membranes after irradiation was measured using an ion selective electrode (ISE) (Mettler-Toledo, ISE part no. 51340510, meter model number MX300), which was calibrated for the range 0.01−1000 ppm fluoride using aqueous solutions of NaF. The ISE was immersed in a solution containing 20 mL of sample and 20 mL of TISAB II solution with constant stirring and the potentiometric reading recorded at RT after equilibrium was reached (typically 5−10 min). Fluoride concentration data are reported against the calibration curve. The detection accuracy limit is ~0.1 ppm (corresponding to 5.26×10^{-6} M).

Ion Exchange Capacity (IEC). The ion exchange capacity was determined by acid−base titration using a Metrohm 848 Titrino Plus titrator. Membranes were soaked in 2 M NaCl solution for 12 h before titrating with 0.01 M NaOH. The samples (in their Na^+ form) were dried after titration in a vacuum oven at 110 °C for 12 h. Ion exchange capacities (IEC, mmol/g) are given in units of mmoles of titratable protons per gram dry weight of ionomer:

$$\mathrm{IEC} = \frac{V_{\mathrm{NaOH}} \times M_{\mathrm{NaOH}}}{W_{\mathrm{dry}}}$$

where V_{NaOH} and M_{NaOH} are the blank-corrected volume [mL] and molar concentration [mol/L] of NaOH solution, respectively. W_{dry} is the dry weight of the membrane in H^+ form [g].

Water Uptake. The membranes were soaked in deionized water at 25 °C for 24 h (where the water was exchanged every 4 h) and blotted with a Kim wipe to remove surface water prior to determining the "wet" weight (W_{wet}). The "dry" weight (W_{dry}) was obtained after heating the membrane at 110 °C for 12 h under vacuum.

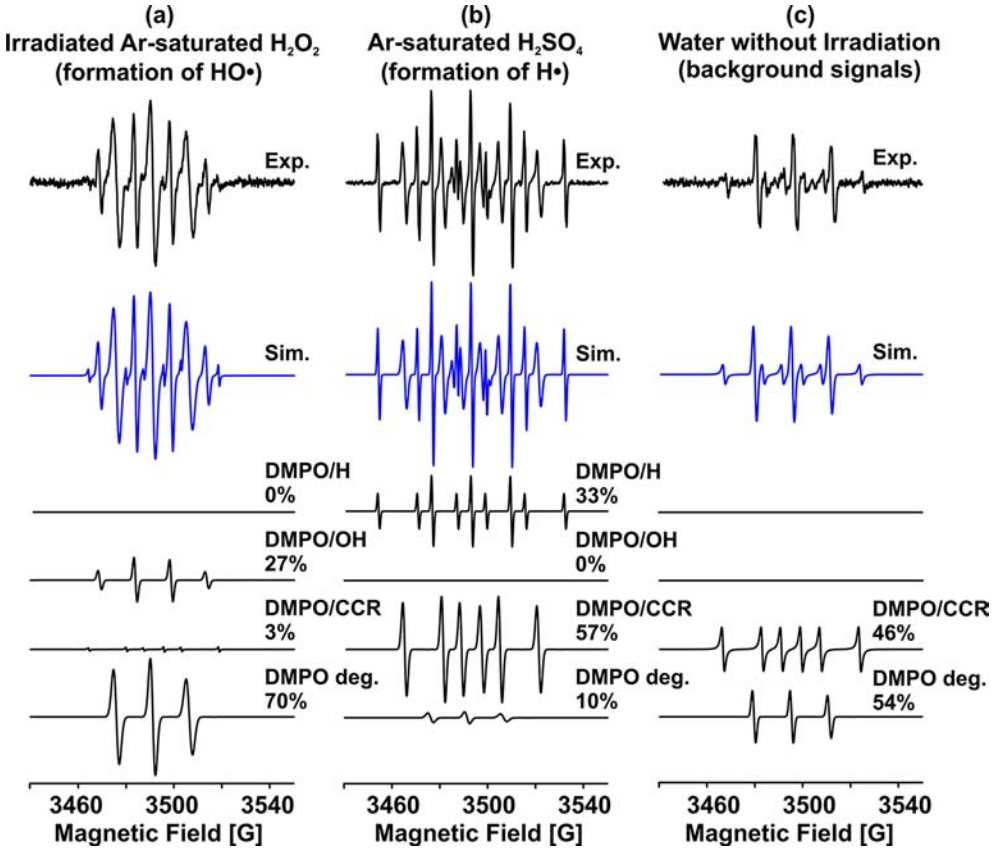

Figure 4. ESR spectra of DMPO adducts detected in (a) irradiated Ar-saturated H_2O_2 (10 vol%); (b) irradiated Ar-saturated 0.01 M H_2SO_4/1 M *t*-BuOH; and (c) DMPO in water prior to irradiation.

Table 1. Hyperfine Splitting and *g* Values of DMPO Adducts Detected

		hyperfine splitting [G]			
samples	adduct	a_N	a_H	*g* value	relative intensity [%]
Ar-saturated H_2O_2 (240 kGy)	DMPO/OH	14.8	15.0	2.0057	27
	DMPO/CCR	15.4	23.0	2.0037	3
	DMPO deg.	14.8		2.0040	70
Ar-saturated H_2SO_4 (240 kGy)	DMPO/H	16.4	22.4 (2H)[a]	2.0067	33
	DMPO/CCR	15.6	23.0	2.0037	57
	DMPO deg.	15.0		2.0040	10
Water (No Irradiation)	DMPO/CCR	15.4	23.0	2.0037	46
	DMPO deg.	14.8		2.0040	54

[a]There are 2 hydrogen in this position.

$$\text{Water Uptake} = \frac{W_{wet} - W_{dry}}{W_{dry}} \times 100$$

Proton Conductivity. In-plane proton conductivity was measured by AC impedance spectroscopy with a Solartron 1260 frequency response analyzer (FRA) employing a two-electrode configuration, according to a procedure described elsewhere.[53] Proton conductivity (σ_{H+}) of fully hydrated membranes was measured at RT by placing a membrane (~10 mm × 5 mm) between two Pt electrodes of a conductivity cell and applying a 100 mV sinusoidal AC voltage over a frequency range of 10 MHz to 100 Hz. Proton resistance was obtained from the high-frequency intercept of the complex impedance with the real axis, R_{H+} [Ω], from which proton conductivity was calculated using the distance between electrodes, *L* [cm], and cross-sectional area of the membrane, *A* [cm^2]:

$$\sigma_{H^+} = \frac{L}{A \cdot R_{H^+}}$$

RESULTS

Selective Radical Generation by E-Beam Irradiation of Aqueous Solutions. Ar-saturated aqueous solutions of H_2O_2 and Ar-saturated aqueous acidic solutions (pH 2) were irradiated with an e-beam as described. In order to determine which radicals were generated, ESR spectroscopy was performed on the solutions irradiated in the presence of the spin trap, DMPO. Experimental and simulated ESR spectra of the radical adducts are presented in Figure 4. The relative intensities and the corresponding magnetic parameters are summarized in Table 1.

While the relative intensities of the adducts do not necessarily provide a quantifiable correlation with the radicals that are formed because of the different trapping rates of DMPO with the different radicals in the mixture,[54,55] speciation is highly reliable due to the position and hyperfine splitting of

dx.doi.org/10.1021/ja408032p | J. Am. Chem. Soc. 2013, 135, 15923−15932

the signals. The DMPO/OH spectrum is characterized by a *g*-factor of 2.0057, splitting by one ^{14}N (a_N = 14.8 G) and one ^{1}H (a_H = 15.0 G) nuclei, respectively (see Supporting Information, Figure S3-a). The DMPO/H spectrum is characterized by a *g*-factor of 2.0067, splitting by one ^{14}N (a_N = 16.4 G) and by two equivalent ^{1}H (a_H = 22.4 G) nuclei, respectively (see Supporting Information, Figure S3-b). As observed in Figure 4, DMPO/HO adducts are detected in irradiated Ar-saturated H_2O_2 solutions, but DMPO/H is not; whereas DMPO/H adducts are detected in irradiated Ar-saturated acid solutions but DMPO/HO is not, indicating exclusive formation of HO$^\bullet$ and H$^\bullet$, respectively. In addition to DMPO adducts of HO$^\bullet$ and H$^\bullet$ radicals, two other adducts were consistently detected. These two signals were also present in the ESR spectrum of DMPO in water prior to irradiation, as shown in Figure 4-c, and are due to a DMPO adduct possessing a carbon centered radical (DMPO/CCR: a_N = 15.4 G, a_H = 23.0 G); and an impurity due to decomposed DMPO (DMPO.deg: $a_N \sim 15$ G). The source of carbon centered radicals (DMPO/CCR) is believed due to hydrolysis of DMPO, as reported in the literature;[36,56−59] the latter signal is due to N−C bond cleavage and ring-opening.[36,56,57,60] The mechanism of DMPO degradation is provided in Scheme S2 in the Supporting Information. In the present study, it is sufficient to recognize that these signals are not due to the e-beam irradiation but, rather, background signals.

By distinguishing the background signals from signals due to the formation of new spin adducts, the sole formation of HO$^\bullet$ radicals in irradiated H_2O_2 solutions is established by the sole presence of the DMPO/OH adduct (Figure 4-a) and the sole formation of H$^\bullet$ radicals in irradiated 0.01 M H_2SO_4 solution is established by the sole formation of the DMPO/H adduct. Note that since the H$^\bullet$ radical can react with water to form HO$^\bullet$ (H$^\bullet$+ $H_2O \rightarrow$ HO$^\bullet$ + H_2), it was necessary to add *t*-BuOH to scavenge HO$^\bullet$[40,42] and form a stable and comparatively unreactive carbon center radical: $C(CH_3)_3-OH + HO^\bullet \rightarrow (^\bullet CH_2)-C(CH_3)_2-OH + H_2O$ ($k = 6.0 \times 10^8$ L.mol^{-1} s^{-1}). The signal of this radical overlaps that of the DMPO/CCR adduct formed from DMPO degradation, and hence the intensity of the DMPO/CCR adduct in Ar-saturated acid (containing *t*-BuOH) is higher than in its absence. Increasing concentrations of *t*-BuOH were employed in order to quench the HO$^\bullet$ radical. We found that 0.5 M *t*-BuOH, as suggested in earlier work,[39] was not sufficient to capture all HO$^\bullet$ radicals: we therefore used 1 M *t*-BuOH for the exclusive production of H$^\bullet$ radical (Figure 4-b). A comparison of ESR spectra of DMPO adducts in Ar-saturated acid with 0.5 and 1 M *t*-BuOH is shown in Figure S1 of Supporting Information, demonstrating the need to use 1 M *t*-BuOH.

Solid State NMR of Nafion Membranes. MAS ^{19}F NMR spectroscopy was used to detect changes in ionomer structure after exposure to H$^\bullet$ and HO$^\bullet$. Figure 5 presents the spectra of pristine Nafion 211. Peak assignments are based on a previous analysis.[61] Peak positions, line shapes, and error margins are shown in Table 2.

The most intense signal occurs at −122 ppm which is an overlap of different signals due to main chain CF_2 units. The difference in chemical shift values and line broadenings of the deconvoluted spectra result from the varied distance of CF_2 units from the branch point.[34,61] The ^{19}F resonance at −138 ppm is assigned to the CF group in the ionomer backbone to which the side chain is attached, CF(m). The CF group in the side chain, CF(s), appears at −144 ppm; the SCF_2 group

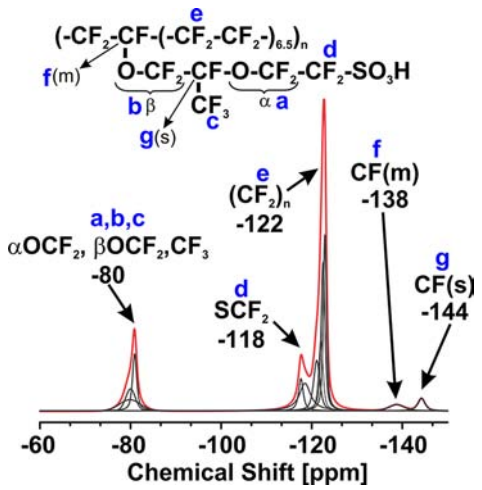

Figure 5. Solid state ^{19}F NMR spectrum (red line) and peak assignment of Nafion 211. The deconvoluted spectrum is shown in black.

Table 2. Deconvoluted ^{19}F NMR Signals for Pristine Nafion 211

signal	position [ppm]	relative area	width [kHz]	G/L[a]
β-OCF_2	−79.9	2	2.01 (±0.2)	1
α-OCF_2	−80.0	2	0.95 (±0.1)	1
CF_3	−80.9	3	0.41 (±0.03)	0.3
SCF_2	−117.6	2	0.46 (±0.04)	0.8
CF_2 (n)	−118.5	4	1.13 (±0.2)	0
	−121.1	4	0.61 (±0.1)	0.4
	−122.0	4	0.43 (±0.08)	0.4
	−122.5	8	0.38 (±0.06)	0.4
	−122.9	8	0.32 (±0.06)	0.4
CF(m)	−138.8	1	1.47 (±0.05)	0.3
CF(s)	−144.2	1	0.7 (±0.02)	0.6

[a]G/L: Gaussian:Lorentzian ratio in peak shape. For assignments see Figure 5.

appears at −118 ppm, and the two OCF_2 groups and the CF_3 group of the side chain overlap at −80 ppm. Deconvoluting the signal at −80 ppm into 3 peaks with relative areas of 2:2:3 reveals the OCF_2 groups (two signals with similar area) and CF_3 group (the peak with the larger area). Based on the expected mobility of these groups, the narrower peak is assigned to OCF_2 near the end of the side chain (α-OCF_2) and the broader signal to the OCF_2 near the branch point (β-OCF_2), in agreement with reported $^{19}F-^{13}C$ 2D NMR analyses of Nafion 117.[61]

The absolute fluorine content associated with each fluorine-containing unit before and after exposure to HO$^\bullet$ and H$^\bullet$ is shown in Figure 6-a, and the percentage loss in fluorine content is shown in Figure 6-b. For Nafion 211 exposed to HO$^\bullet$ radicals the concentration of main chain CF_2 units (the sum of 5 peaks with the estimation error ±1.5%) was unchanged. Also, no change was observed in the main chain CF content at −144 ppm, confirming that the main chain of the polymer is unaltered by HO$^\bullet$. In contrast, the side chain clearly degrades. The largest change in fluorine content was observed for the side chain SCF_2 and α-OCF_2 groups, which decreased by ∼16.5% (see Figure 6-b). The CF side chain group concentration decreased by 13%, similar to the change in CF_3 content (13%). A smaller change was observed for the β-OCF_2 groups (10.9%).

dx.doi.org/10.1021/ja408032p | J. Am. Chem. Soc. 2013, 135, 15923−15932

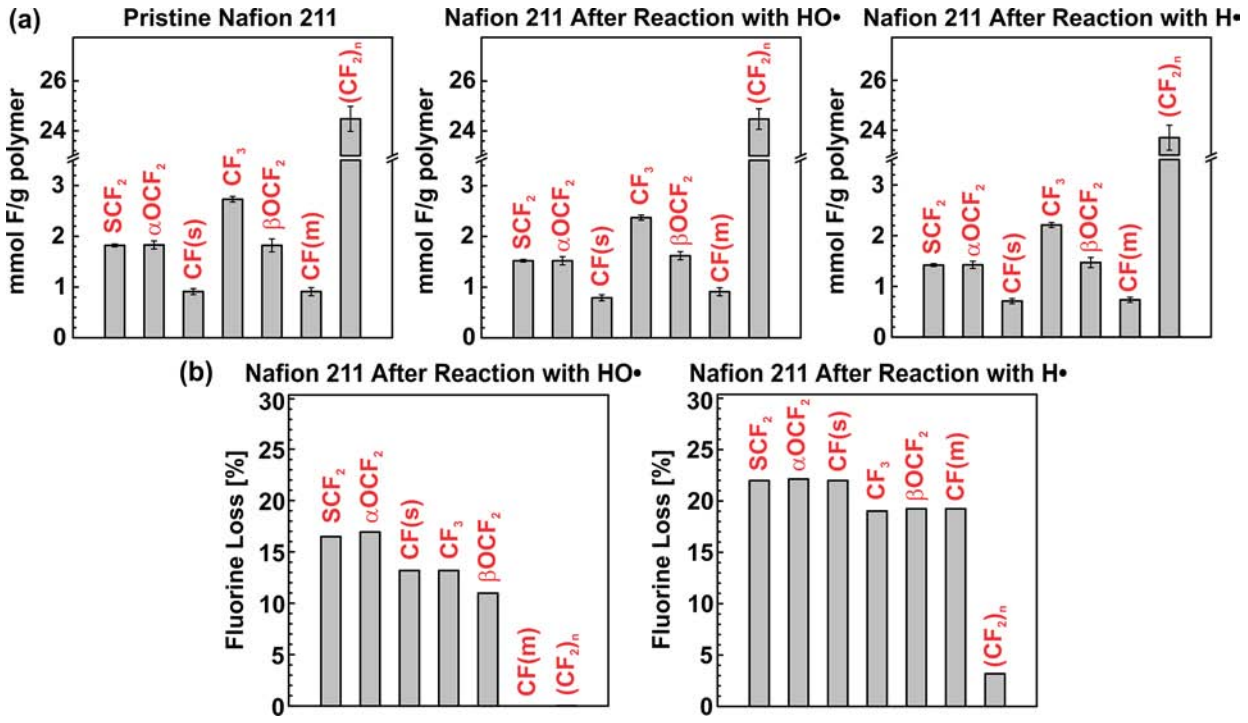

Figure 6. (a) Fluorine concentration and (b) fluorine loss associated with each fluorine-containing unit in Nafion 211 before and after exposure to H• and HO• radicals. The error margins of the data in (b) are similar to those in (a).

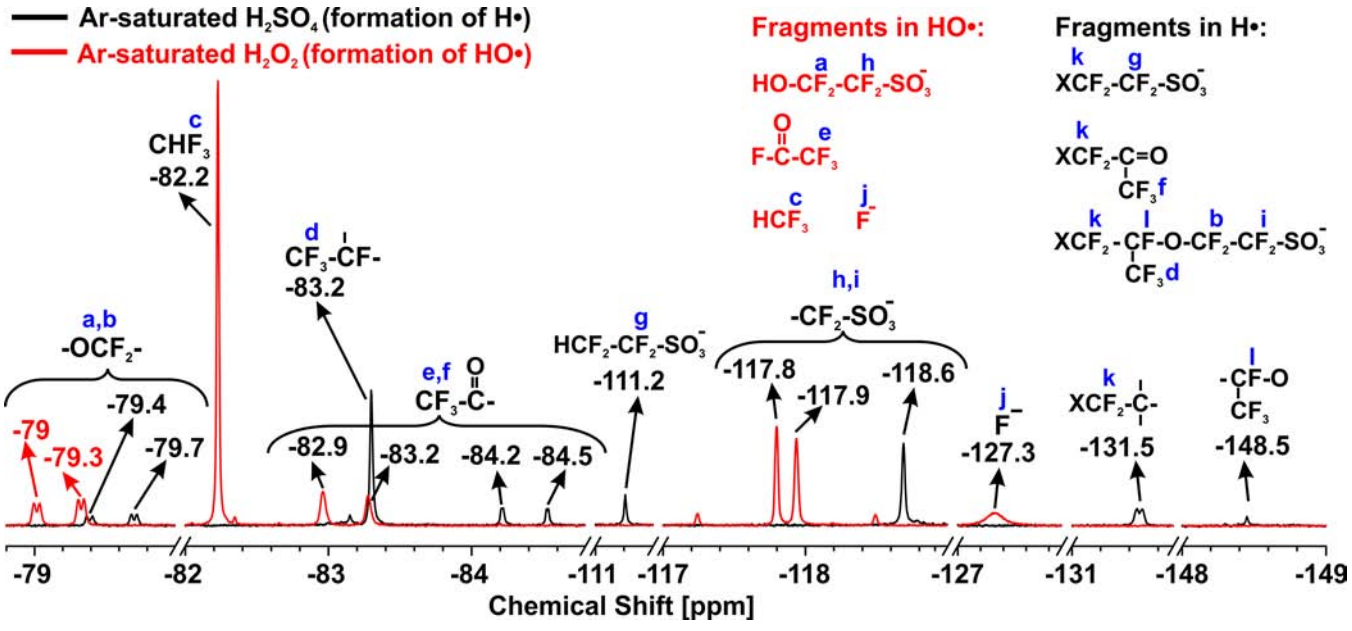

Figure 7. ^{19}F NMR spectra of isopropyl alcohol-soluble residues after exposure of Nafion 211 to H• (black lines) and HO• (red lines). Peak assignments and proposed fragments are indicated.

For Nafion 211 exposed to H• radicals, the changes in fluorine content were larger and different in nature. The SCF_2, α-OCF_2, and CF(s) groups decreased at the same rate (~22% fluorine loss). The changes in other side chain units, including CF_3, β-OCF_2, were slightly lower than this (~19%). A significant decrease was observed in the main chain CF(m) content (19.2%), similar to that observed for the decrease in CF_3 and β-OCF_2 groups, yet the decrease in main chain CF_2 content was much smaller (3%). This is strong evidence that, in contrast to HO•, H• attacks the main chain, and more specifically, the main chain CF(m) branch point.

NMR Spectroscopy of Solution and Solid Residues. As described in the Experimental Section, the solutions of membranes exposed to H• and HO• were freeze-dried and dissolved in IPA. ^{19}F NMR spectra of the IPA-soluble compounds are shown in Figure 7.

Exposure of Nafion to H• also yielded an IPA-insoluble residue, which was subsequently analyzed by MAS ^{19}F NMR spectroscopy (see Figure 8).

dx.doi.org/10.1021/ja408032p | J. Am. Chem. Soc. 2013, 135, 15923−15932

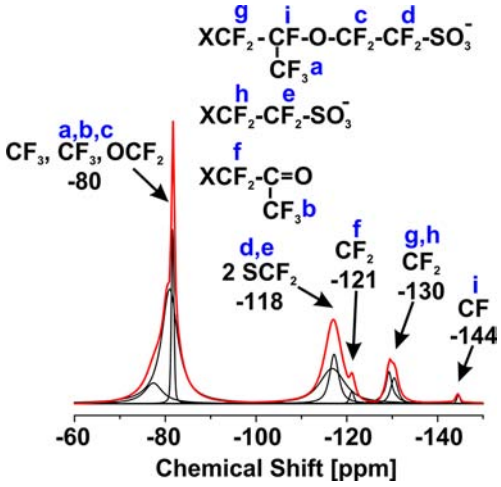

Figure 8. Solid state ^{19}F NMR spectrum of solid residues in solution upon exposure of Nafion 211 to H$^{\bullet}$. Peak assignments and proposed fragments are indicated. For more information on spectra deconvolution see Figure S4 in Supporting Information.

NMR spectra of IPA-soluble residues from HO$^{\bullet}$ radical attack yield a signal at −127.3 for the fluoride ion, most likely due to dissociation of HF, as previously proposed for the soluble species of membranes exposed to Fenton's reagent.[18,27,31] Signals at ∼−118 ppm and ∼−80 ppm attributed to fluorine next to SO_3^- and O−C indicate the presence of $-OCF_2CF_2SO_3^-$ fragments, consistent with the solid state NMR data, which reveal a decrease in concentration of side chain SCF_2 and OCF_2 groups. Peaks at −82.2, −82.9, and −83.2 are due to CF_3 units having different neighboring groups. The strong peak at −82.2 ppm is assigned to fluorine in CHF_3.

The IPA-soluble residues of membrane exposed to H$^{\bullet}$ provide different signals to the HO$^{\bullet}$ reaction analogue. For instance, the signal for F^- is completely absent, and in addition to OCF_2 and SCF_2 signals at ∼−80 ppm and −118.6 ppm, new signals due to CF_3 (−83.2, −84.2, −84.5), CF_2 (−131.5), and CF (−148.5) are observed. The signal at −111.2 ppm is due to SCF_2 signal in $HCF_2-CF_2-SO_3^-$.

MAS ^{19}F NMR of the solid residue of Nafion 211 after exposure to H$^{\bullet}$ radicals is presented in Figure 8. The spectra possesses a number of peaks similar to that of the pristine Nafion spectra shown in Figure 5, providing evidence that the residues contain large fragments of the ionomer. However, there are differences: the signal at ∼−118 is an overlap of 2 signals with different line widths (−116.8 and −117.2 ppm; with the line width of 6.67 and 2.35 Hz, respectively). The position of both peaks confirms the assignment of SCF_2 groups, but the presence of 2 peaks suggest the possibility for having more than one compound. The narrow and broad peak could be due to the SCF_2 group attached to a small and larger molecular structure, respectively. The signal at −80 ppm is assigned to OCF_2 and CF_3 groups, but the relative ratio of the peaks is different from that found in pristine Nafion. The signal at −130 ppm is also an overlap of 2 signals which are not present in Nafion. These peaks, and the peak at −121 ppm, are assigned to CF_2 groups in different environments. The peak at −144 ppm is similar to that observed in Nafion and is assigned to CF in the side chain.

ATR-FTIR Spectroscopy. The respective FTIR spectra of the Nafion samples before and after exposure to H$^{\bullet}$ and HO$^{\bullet}$ are shown in Supporting Information, Figure S5, together with the peak assignments.[62] A comparison of the spectra before and after chemical degradation show a general decrease in intensity of the C−O−C (960 and 980 cm^{-1}), S−C (805 cm^{-1}), and S−O (1056 cm^{-1}) stretching modes, similar to other reports on ATR-FTIR of Nafion treated with Fenton's reagent.[31] At the same time, an intensity decrease is detected for peaks at 1132 and 1196 cm^{-1} related to the stretching modes of CF groups. The appearance of two new peaks upon exposure to H$^{\bullet}$ and HO$^{\bullet}$ (1628 and 1692 cm^{-1}) is attributed to C═O stretching modes, resulting from the formation of carbonyl or carboxylic acid groups.[38,63]

Effect of H$^{\bullet}$ and HO$^{\bullet}$ on Membrane Properties. The membranes remained colorless after exposure to radicals, were homogeneously smooth, but mechanically more fragile. Table 3 lists the fluoride ion release, together with selected membrane properties. The IEC decreased by 20.9% and 16.5% after exposure to H$^{\bullet}$ and HO$^{\bullet}$, respectively. These values are consistent with that calculated from ^{19}F NMR data. Water uptake and proton conductivity decreased commensurate with loss of IEC. Fluoride ion release, which is presumed to be due to HF loss,[18,27,31,64] for the membranes exposed to H$^{\bullet}$ is almost half that of the membranes exposed to HO$^{\bullet}$.

Table 3. Fluoride Release, Ion Exchange Capacity (IEC), Water Uptake, And Proton Conductivity (σ_{H+}) of Nafion 211 after Exposure to H$^{\bullet}$ and HO$^{\bullet}$

radical	F^- release [mmol/g]	IEC [mmol/g]	H_2O uptake [%][b]	σ_{H+} [S/cm]
[a]		0.91 ± 0.01	35 ± 1	0.079 ± 0.001
HO$^{\bullet}$	0.51	0.76 ± 0.01	21 ± 1	0.059 ± 0.004
H$^{\bullet}$	0.28	0.72 ± 0.05	29 ± 1	0.061 ± 0.003

[a]Pristine Nafion 211. [b]At RT, fully hydrated membrane.

DISCUSSION

Selective Radical Generation. It has long been known that exposure of water to high-energy radiation, such as β-rays and γ-rays, results in the formation of hydrated electrons (e_{aq}^-), which rapidly react with water to generate radicals.[40,50,65,66] The use of γ-rays necessitates long exposure times (3 h for doses of 100 kGy)[39] while similar doses of β-rays require much shorter irradiation times (5 min for 80 kGy using a 10 MeV e-beam source). In addition, employing γ-rays, membranes are invariable exposed to high energy irradiation. In fact γ-rays are commonly used to produce radicals on polymer main chains, allowing for their post modification, for example, the preparation of graft copolymers.[67−71] In contrast, it is relatively straightforward to control the penetration depth of β-rays using aqueous solution so as not to overexpose a substrate. In the configuration used, while hydrated electrons and radicals are produced in the whole depth of liquid exposed to the e-beam, given the short lifetimes of HO$^{\bullet}$ and H$^{\bullet}$ ($t_{1/2}$ = 10^{-9} s and 10^{-7} s, respectively)[72−74] only radicals in the immediate vicinity of the membrane react with the membrane. Hence, it is important to reproducibly control the depth of penetration of the e-beam, which we did so that <2% of the irradiation dose reaches the membrane surface. The fact that different molecular residues and mechanisms are observed in different solutions, and that no degradation was observed when the penetration depth was increased to 6 cm, indicates the observations are not the result of direct irradiation but rather the result of radical reactions. It is important to recognize that the radicals are transient species

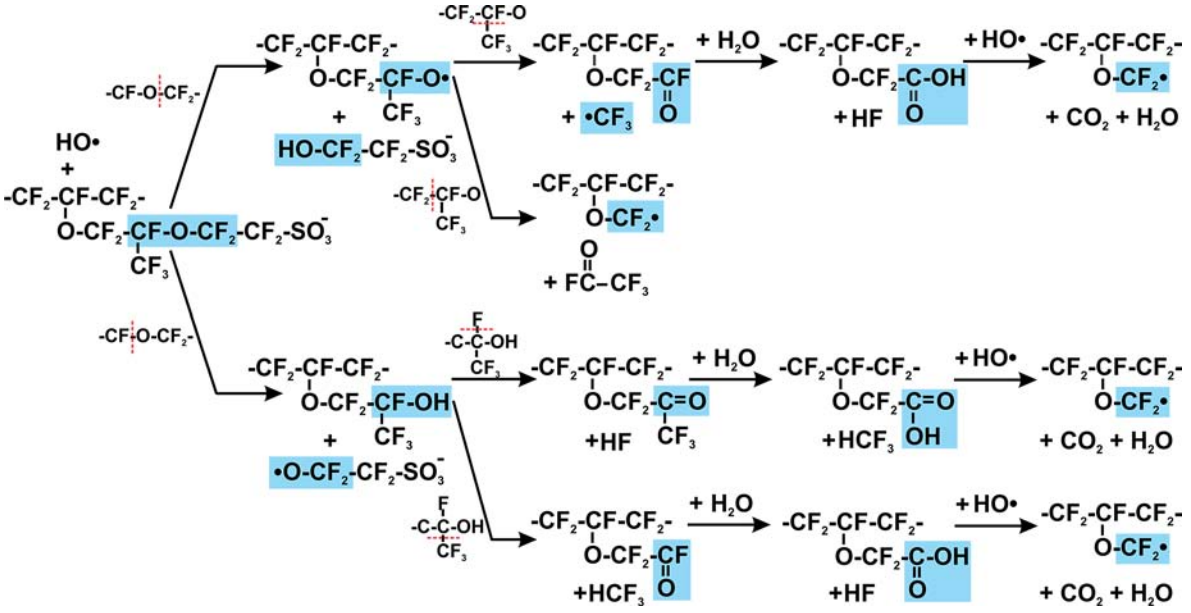

Figure 9. Proposed mechanism of HO• radical attack on Nafion 211.

and are generated in nonuniform concentration near, or at, the membrane surface. It is therefore not possible to quantitatively compare the rates of reaction of H• and HO• with the membranes as the absolute relative concentrations are not known. Nonetheless, qualitative information concerning the mechanism of attack is still possible.

Side Chain vs Main Chain Degradation. Quantified MAS NMR data indicated that no changes in the main chain occurred upon exposure to HO•, at least to the extent that 16.5% of the side chain termini had been lost. This confirms that the attack point by HO• is the side chain and not the main chain. In contrast, upon exposure of Nafion to H•, in addition to a 22% decrease in side chain termini, a 19.2% decrease in the main chain CF(m) units was observed. The changes in the other main chain signals, e.g., CF_2(n), are, however, very small (3%). This supports the assertion that the CF(m) branch point is the main point of attack for H•, and that the CF_2(n) units remain largely unperturbed. The latter point also supports the assertion that the changes in polymer structure observed are not the result of direct β-irradiation but indeed the result of radical reactions.

HO• Radical Generation: β-Irradiation vs Fenton's Reagent. Selective HO• radical generation by β-irradiation provides an alternative, comparative method to Fenton's reagent for radical generation. NMR spectra obtained for Nafion 211 after exposure to HO• generated by β-irradiation are similar to those reported upon exposure to HO• radicals generated by Fenton's reagent.[34] That is, no main chain degradation is observed and side chain degradation is more prevalent close to the ionic head groups rather than near the branch point. The rate of loss of α-OCF_2 and SCF_2 units (16.5% in this study) were similar, indicative of a first point of HO• attack at α-OCF_2, leading to cleavage of -$OCF_2CF_2SO_3^-$ and/or $-CF_2CF_2SO_3^-$. The extent of loss of β-OCF_2 and CF_3 is similar but lower than α-OCF_2. These observations are consistent with the likelihood that HO• radicals continue to attack further up the side chain after cleaving the α-O−C bond (as illustrated in Figure 9).[34] Products such as $HOCF_2CF_2SO_3^-$, $FCOCF_3$, HCF_3, and F^- found in the IPA-soluble residues (Figure 7) are further confirmation of α-OCF_2 bond cleavage, and β-OCF_2 bond cleavage. The formation of C═O was observed by ATR-FTIR. The observed reduction in IEC of the samples determined by titration (16.5%) is exactly the same as that determined by NMR. These observations together with the ^{19}F solid state NMR data lead us to propose a mechanism for HO• attack as illustrated in Figure 9. The suggested mechanism anticipates the formation of $HOCF_2CF_2SO_3^-$, $FCOCF_3$, HCF_3, and F^-, as observed in Figure 7. It is also consistent with experimental work of Danilczuk et al. on the formation of $^{\bullet}OCF_2R$ radicals obtained by spin trapping the model compound, $CF_3CF_2OCF_2CF_2SO_3^-$, degraded by Fenton's reagent,[75] and consistent with the kinetic study of Dreizler et al. on model compounds, in which they conclude the point of attack by HO• radical is the α-O−C bond.[33]

In Figure 9, we suggest that after the first HO• radical attack carboxylic groups are formed on the side chain (as ATR-FTIR also indicates), which primes it for another radical attack causing unzipping of the side chain, similar to the mechanism suggested by Curtin et al. for HO• radical attack on main chain terminal −COOH groups that are present on nonchemically stabilized PFSA ionomers.[23]

Mechanism of H• Radical Attack. There are no prior experimental data in the literature pertaining to the mechanism of H• radical attack on Nafion. The results of ^{19}F solid state NMR in this work reveals that H• attacks the main chain and side chain. H• attack decreases the number of SCF_2, α-OCF_2, and CF(s) groups by the same extent (22%) suggesting these groups are cleaved by a common reaction step. CF_3, β-OCF_2, and CF(m) units are also lost to the same extent as each other (19.2%), also suggesting a common step. These data indicate H• radical attack of C−F bonds in both tertiary carbons (see Figure 6-b). The weakest of the C−F bonds in Nafion PFSA ionomer is indeed the C−F in the side-chain bonded to the ether group and the C−F bond at the branch point in the backbone.[18,25,32] The bond dissociation energy for CF(m) and CF(s) is calculated to be 435.6 and 455.6 kJ/mol, respectively.[76] This information confirms the ^{19}F MAS NMR data of this work suggesting C−F bond attack at both main chain and side chain, with higher possibility of reaction at the

dx.doi.org/10.1021/ja408032p | J. Am. Chem. Soc. 2013, 135, 15923−15932

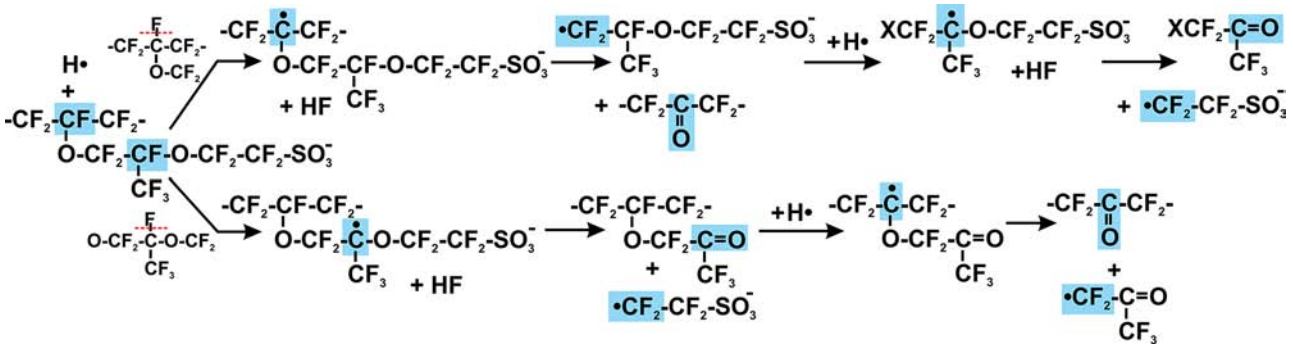

Figure 10. Proposed mechanism of H• radical attack on Nafion 211.

main chain. •CF_2−$CF(CF_3)$−OCF_2−CF_2−SO_3^- produced as a result of H• radical attack on the main chain CF group, whereas •CF_2−CF_2−SO_3^- is produced by attack on the side chain CF group, fragments that are detected by NMR analyses of IPA-soluble and solid residues. The lower fluoride ion release rate observed by ion selective electrode and ^{19}F NMR analyses is consistent with H• generating large fragments of degraded ionomer. A mechanism that accounts for these observations is presented in Figure 10, showing attack of the C−F bond in CF(m) and CF(s) by H•. The mechanism indicates H• cleaves the whole side chain with the formation of only 1 or 2 HF molecules (depending on the reaction pathway), whereas HO• attack forms 3 or 4 HF.

CONCLUSIONS

β-Irradiation of water was proven to yield exclusive formation of HO• and H• radicals. This provides the first opportunity to study membrane degradation in the sole presence of H• and HO•. Exposure of Nafion 211 to HO• or H• radicals led to chemical degradation but via different mechanisms, which was explored by quantitative ^{19}F NMR spectroscopy, ATR-FTIR spectroscopy, ion exchange capacity, water uptake, proton conductivity, and fluoride ion formation. HO• attacks the α-O−C bond in the side chain, involving many reaction steps and high F^- release rates; H• radical attack occurs on the main chain, almost exclusively at the CF branch point, in addition to side chain bond cleavage, causing lower F^- release rates.

ASSOCIATED CONTENT

Supporting Information

ESR spectra of DMPO adducts comparing the effect of HO• radical scavenger in Ar-saturated H_2SO_4 solutions with different concentration and N_2O-saturated H_2O, reaction of DMPO and free radical, ESR signal splitting for DMPO/OH and DMPO/H adducts, DMPO degradation via N−C bond cleavage, ^{19}F NMR spectrum deconvolution of Nafion 211 solid residue upon exposure to H• and ATR-FTIR spectra of Nafion 211 samples before and after exposure to radicals. This material is available free of charge via the Internet at http://pubs.acs.org.

AUTHOR INFORMATION

Corresponding Author

*E-mail: holdcrof@sfu.ca.

Funding

Notes

The authors declare no competing financial interest.

ACKNOWLEDGMENTS

The funding of this research is provided by Automotive Partnership Canada. Special thanks to Prof. Charles Walsby for access to, and assistance with, the ESR spectrometer; Dr. Andrew Lewis for the technical support with solid state NMR; and Ballard Power Systems Inc. for samples of Nafion® 211. The authors also thank Alex English of Iotron Industries Canada/USA Inc. for insightful discussions on the topic of e-beam irradiation.

REFERENCES

(1) Hickner, M. A.; Ghassemi, H.; Kim, Y. S.; Einsla, B. R.; McGrath, J. E. *Chem. Rev.* **2004**, *104*, 4587−4612.
(2) Carle, G.; Axhausen, K. W.; Wokaun, A.; Keller, P. *Transport Reviews* **2005**, *25*, 739−760.
(3) *The US DOE Hydrogen and Fuel Cell Plan*; Washington, D.C., 2010.
(4) Rodgers, M. P.; Bonville, L. J.; Kunz, H. R.; Slattery, D. K.; Fenton, J. M. *Chem. Rev.* **2012**, *112*, 6075−6103.
(5) Huang, X.; Solasi, R.; Zou, Y.; Feshler, M.; Reifsnider, K.; Condit, D.; Burlatsky, S.; Madden, T. *J. Polym. Sci., Part B: Polym. Phys.* **2006**, *44*, 2346−2357.
(6) Surowiec, J.; Bogoczek, R. *J. Thermal Anal.* **1988**, *33*, 1097−1102.
(7) Pozio, A.; Silva, R. F.; De Francesco, M.; Giorgi, L. *Electrochim. Acta* **2003**, *48*, 1543−1549.
(8) Schulze, M.; Wagner, N.; Kaz, T.; Friedrich, K. A. *Electrochim. Acta* **2007**, *52*, 2328−2336.
(9) Aoki, M.; Uchida, H.; Watanabe, M. *Electrochem. Commun.* **2005**, *7*, 1434−1438.
(10) Asano, N.; Aoki, M.; Suzuki, S.; Miyatake, K.; Uchida, H.; Watanabe, M. *J. Am. Chem. Soc.* **2006**, *128*, 1762−1769.
(11) Kinumoto, T.; Inaba, M.; Nakayama, Y.; Ogata, K.; Umebayashi, R.; Tasaka, A.; Iriyama, Y.; Abe, T.; Ogumi, Z. *J. Power Sources* **2006**, *158*, 1222−1228.
(12) Liu, W.; Ruth, K.; Rusch, G. *J. New Mater. Electrochem. Syst.* **2001**, *4*, 227−232.
(13) Mittal, V. O.; Kunz, H. R.; Fenton, J. M. *J. Electrochem. Soc.* **2006**, *153*, A1755−a1759.
(14) Mittal, V. O.; Kunz, H. R.; Fenton, J. M. *Electrochem. Solid State Lett.* **2006**, *9*, A299−A302.
(15) Mittal, V. O.; Kunz, H. R.; Fenton, J. M. *J. Electrochem. Soc.* **2007**, *154*, B652−B656.
(16) Balko, E. N.; Chaklos, J. T. *J. Appl. Polym. Sci.* **1981**, *26*, 1519−1531.
(17) Danilczuk, M.; Coms, F. D.; Schlick, S. *J. Phys. Chem. B* **2009**, *113*, 8031−8042.
(18) Ghassemzadeh, L.; Kreuer, K.-D.; Maier, J.; Müller, K. *J. Phys. Chem. C* **2010**, *114*, 14635−14645.
(19) Gubler, L.; Dockheer, S. M.; Koppenol, W. H. *J. Electrochem. Soc.* **2011**, *158*, B755−B769.
(20) Okada, T.; Satou, H.; Yuasa, M. *Langmuir* **2003**, *19*, 2325−2332.

(21) Xie, J.; Wood, D. L.; More, K. L.; Atanassov, P.; Borup, R. L. *J. Electrochem. Soc.* **2005**, *152*, A1011−A1020.
(22) Endoh, E. *Electrochem. Solid State Lett.* **2004**, *7*, A209−A211.
(23) Curtin, D. E.; Lousenberg, R. D.; Henry, T. J.; Tangeman, P. C.; Tisack, M. E. *J. Power Sources* **2004**, *131*, 41−48.
(24) Zhou, C.; Guerra, M. A.; Qiu, Z. M.; Zawodzinski, T. A.; Schiraldi, D. A. *Macromolecules* **2007**, *40*, 8695−8707.
(25) Coms, F. D. *ECS Trans.* **2008**, *16*, 235−255.
(26) Yu, T. H.; Liu, W.-G.; Sha, Y.; Merinov, B. V.; Shirvanian, P.; Goddard, W. A., III *J. Membr. Sci.* **2013**, *437*, 276−285.
(27) Healy, J.; Hayden, C.; Xie, T.; Olson, K.; Waldo, R.; Brundage, A.; Gasteiger, H.; Abbott, J. *Fuel Cells* **2005**, *5*, 302−308.
(28) Kadirov, M. K.; Bosnjakovic, A.; Schlick, S. *J. Phys. Chem. B* **2005**, *109*, 7664−7670.
(29) Bosnjakovic, A.; Kadirov, M. K.; Schlick, S. *Res. Chem. Intermed.* **2007**, *33*, 677−687.
(30) Ghassemzadeh, L.; Marrony, M.; Barrera, R.; Kreuer, K. D.; Maier, J.; Müller, K. *J. Power Sources* **2009**, *186*, 334−338.
(31) Ghassemzadeh, L.; Kreuer, K. D.; Maier, J.; Müller, K. *J. Power Sources* **2011**, *196*, 2490−2497.
(32) Yu, T. H.; Sha, Y.; Liu, W.-G.; Merinov, B. V.; Shirvanian, P.; Goddard, W. A. *J. Am. Chem. Soc.* **2011**, *133*, 19857−19863.
(33) Dreizler, A. M.; Roduner, E. *Fuel Cells* **2012**, *12*, 132−140.
(34) Ghassemzadeh, L.; Holdcroft, S. *J. Am. Chem. Soc.* **2013**, *135*, 8181−8184.
(35) Bosnjakovic, A.; Schlick, S. *J. Phys. Chem. B* **2004**, *108*, 4332−4337.
(36) Bosnjakovic, A.; Schlick, S. *J. Phys. Chem. B* **2006**, *110*, 10720−10728.
(37) Akiyama, Y.; Sodaye, H.; Shibahara, Y.; Honda, Y.; Tagawa, S.; Nishijima, S. *Polym. Degrad. Stab.* **2010**, *95*, 1−5.
(38) Akiyama, Y.; Sodaye, H.; Shibahara, Y.; Honda, Y.; Tagawa, S.; Nishijima, S. *J. Power Sources* **2010**, *195*, 5915−5921.
(39) Uegaki, R.; Akiyama, Y.; Tojo, S.; Honda, Y.; Nishijima, S. *J. Power Sources* **2011**, *196*, 9856−9861.
(40) Buxton, G. V.; Greenstock, C. L.; Helman, W. P.; Ross, A. B. *J. Phys. Chem. Ref. Data* **1988**, *17*, 513−886.
(41) Sternheim, M. M.; KanSternheim, M. M.; Kane, J. W. *General Physics*; John Wiley & Sons: New York, 1986.
(42) Christensen, H.; Sehested, K. *J. Phys. Chem.* **1986**, *90*, 186−190.
(43) Rogers, D. W. O.; Bielajew, A. F. In *Monte Carlo Transport of Electrons and Photons*; Jenkins, T. M., Nelson, W. R., Rindi, A., Nahum, A. E., Rogers, D. W. O., Eds.; Plenum Press: New York, 1988; pp 139−152.
(44) The Sub-Committee on Radiation, D. *Phys. Med. Biol.* **1966**, *11*, 505.
(45) ICRU *Radiation Dosimetry: Electron Beams with Energies between 1 and 50 MeV*; Report *35*; ICRU: Washington, D.C., 1984.
(46) Lagercrantz, C. *J. Phys. Chem.* **1971**, *75*, 3466.
(47) Janzen, E. G. *Acc. Chem. Res.* **1971**, *4*, 31.
(48) Janzen, E. G.; Liu, J. I. P. *J. Magn. Reson.* **1973**, *9*, 510−512.
(49) Harbour, J. R.; Chow, V.; Bolton, J. R. *Can. J. Chem.* **1974**, *52*, 3549−3553.
(50) Sargent, F. P.; Gardy, E. M. *Can. J. Chem.* **1976**, *54*, 275−279.
(51) Finkelstein, E.; Rosen, G. M.; Rauckman, E. J.; Paxton, J. *Mol. Pharmacol.* **1979**, *16*, 676−685.
(52) Massiot, D.; Fayon, F.; Capron, M.; King, I.; Le Calvé, S.; Alonso, B.; Durand, J.-O.; Bujoli, B.; Gan, Z.; Hoatson, G. *Magn. Reson. Chem.* **2002**, *40*, 70−76.
(53) Xie, Z.; Song, C. J.; Andreaus, B.; Navessin, T.; Shi, Z. Q.; Zhang, J. J.; Holdcroft, S. *J. Electrochem. Soc.* **2006**, *153*, E173−E178.
(54) Villamena, F. A.; Hadad, C. M.; Zweier, J. L. *J. Phys. Chem. A* **2003**, *107*, 4407−4414.
(55) Villamena, F. A.; Hadad, C. M.; Zweier, J. L. *J. Phys. Chem. A* **2005**, *109*, 1662−1674.
(56) Buettner, G. R.; Oberley, L. W. *Biochem. Biophys. Res. Commun.* **1978**, *83*, 69−74.
(57) Buettner, G. R. *Free Radic. Biol. Med.* **1987**, *3*, 259−303.
(58) Kalyanaraman, B.; Janzen, E. G.; Mason, R. P. *J. Biol. Chem.* **1985**, *260*, 4003−4006.
(59) Rehorek, D.; Janzen, E. G. *Polyhedron* **1984**, *3*, 631−634.
(60) Hawkins, C. L.; Davies, M. J. *Biochem. J.* **1999**, *340*, 539−548.
(61) Chen, Q.; Schmidt-Rohr, K. *Macromolecules* **2004**, *37*, 5995−6003.
(62) Di Noto, V.; Gliubizzi, R.; Negro, E.; Pace, G. *J. Phys. Chem. B* **2006**, *110*, 24972−24986.
(63) Danilczuk, M.; Lancucki, L.; Schlick, S.; Hamrock, S. J.; Haugen, G. M. *ACS Macro Lett.* **2012**, *1*, 280−285.
(64) Curtin, D. E.; Lousenberg, R. D.; Henry, T. J.; Tangeman, P. C.; Tisack, M. E. *J. Power Sources* **2004**, *131*, 41−48.
(65) Uri, N. *Chem. Rev.* **1952**, *50*, 375−454.
(66) Pikaev, A. K.; Ershov, B. G. *Russ. Chem. Rev.* **1967**, *36*, 602−620.
(67) Buchi, F. N.; Gupta, B.; Haas, O.; Scherer, G. G. *Electrochim. Acta* **1995**, *40*, 345−353.
(68) Holmberg, S.; Lehtinen, T.; Nasman, J.; Ostrovskii, D.; Paronen, M.; Serimaa, R.; Sundholm, F.; Sundholm, G.; Torell, L.; Torkkeli, M. *J. Mater. Chem.* **1996**, *6*, 1309−1317.
(69) Chuy, C.; Basura, V. I.; Simon, E.; Holdcroft, S.; Horsfall, J.; Lovell, K. V. *J. Electrochem. Soc.* **2000**, *147*, 4453−4458.
(70) Gubler, L.; Prost, N.; Gürsel, S. A.; Scherer, G. G. *Solid State Ionics* **2005**, *176*, 2849−2860.
(71) Gursel, S. A.; Gubler, L.; Gupta, B.; Scherer, G. G. In *Fuel Cells I*; Scherer, G. G., Ed.; 2008; Vol. *215*, pp 157−217.
(72) Roots, R.; Okada, S. *Radiat. Res.* **1975**, *64*, 306−320.
(73) Sies, H. *Eur. J. Biochem.* **1993**, *215*, 213−219.
(74) Pryor, W. A. *Annu. Rev. Physiol.* **1986**, *48*, 657−667.
(75) Danilczuk, M.; Coms, F. D.; Schlick, S. *Fuel Cells* **2008**, *8*, 436−452.
(76) Tokumasu, T.; Ogawa, I.; Koyama, M.; Ishimoto, T.; Miyamoto, A. *ECS Trans.* **2009**, *25*, 765−772.